Stepwise Multi-Temperature Thermogravimetric Analysis (SMT-TGA) for Rapid Alloy Development

Daniel Monceau, Hugo Enjalbert, Clara Desgranges, Tom Sanviemvongsak, Antoine Casadebaigt, Thomas Perez

High Temperature Corrosion of Materials
https://doi.org/10.1007/s11085-024-10273-8

ORIGINAL PAPER

Stepwise Multi-Temperature Thermogravimetric Analysis (SMT-TGA) for Rapid Alloy Development

Daniel Monceau[1] · Hugo Enjalbert[1] · Clara Desgranges[2] · Tom Sanviemvongsak[1,3] · Antoine Casadebaigt[1,4] · Thomas Perez[1,3]

Received: 11 July 2024 / Revised: 11 July 2024 / Accepted: 20 July 2024

Abstract

A stepwise multi-temperature thermogravimetric analysis (SMT-TGA) method is a rapid and time- and material-efficient measurement procedure for oxidation kinetics over a wide range of temperatures. It is suitable for alloy design and material selection procedures. It involves subjecting a sample to a series of steps at increasing temperatures, followed by steps at decreasing temperatures to identify possible effects on the evolution of oxide layer microstructures on oxidation kinetics. This method has been tested for a wide range of metallic alloys in the present work, allowing for the mapping of possible ranges of parabolic oxidation kinetics of industrial alloys between 600 and 1300°C. Two examples of effects of thermal history have also been described in this publication.

✉ Daniel Monceau
daniel.monceau@toulouse-inp.fr

Hugo Enjalbert
hugo.enjalbert@toulouse-inp.fr

Clara Desgranges
clara.desgranges@cea.fr

Tom Sanviemvongsak
tom.sanviemvongsak@safrangroup.com

Antoine Casadebaigt
antoine.casadebaigt@lasalys.com

Thomas Perez
thomas.perez@safrangroup.com

[1] CIRIMAT Laboratory, University of Toulouse, INPT-ENSIACET, 4 allée Emile Monso, 31030 Toulouse, France

[2] CEA, Université Paris-Saclay, Gif-sur-Yvette, France

[3] Present Address: Present address: Safran Tech, Rue des Jeunes Bois, Châteaufort, CS 80112, 78772 Magny-Les-Hameaux, France

[4] Present Address: Present address: Lasalys, 1 avenue du Champ de Mars, 45100 Orléans, France

Published online: 14 August 2024

Keywords Thermogravimetry · Alloy design · Oxidation kinetics

Introduction

In a context of accelerated alloy development, methodologies of numerical alloy design inserted in the integrated computing materials (ICME) methodology [1, 2] ask for high throughput characterization of new materials [3–5]. When it comes to high-temperature oxidation, obtaining an Arrhenius plot of the parabolic kinetic constant with a single piece of alloy, and in an automated way, is certainly useful. Over the past years, a method has been tested where a piece of alloy is subjected to a succession of high-temperature dwells. This has been done with several types of materials: pure Fe, pure Ni [6], Ti-alloys [7], chromia [8] and alumina [9] forming superalloys and high-entropy alloys. This became achievable due to the method of calculating the parabolic constant following any transient oxidation regime [6]. The method was recently termed "Stepwise Multi-Temperature Thermogravimetric Analysis (SMT-TGA)" [9], and proved to be successful. Nonetheless, certain challenges arose and are addressed in this paper.

Experimental Procedures

The chemical compositions of the metals and alloys used in this study are given in Table 1. Pure Ni, Cr, and Fe were provided by MRC, Praxair, and GoodFellow, respectively. Wrought 718 is detailed in [10] and Ti-6Al-4V in [11]. FeCrAlY ODS alloy PM2000 was provided by Plansee. Some chromia-forming HEA alloys under development were tested, and they are named F, G, and H. Ni-base superalloys AM1 [9], R77, and DS200-Hf alloys were supplied by Safran Aircraft Engines. AMS20 is a Ni-base alumina-forming superalloy under development, AMS20-S was desulfirized by ONERA, CMSX-4 SLS, AMS19, GOL1, GOL2, AD730, and ST201 were provided by Safran Tech, and alloys A, B, C, D, and E are new Ni-base alumina-forming alloys under development.

Specimens as pure Ni, pure Fe, pure Cr, HEA alloys, Ni-base superalloys AM1, AMS19, AMS20, GOL1, GOL2, AD730, ST201, DS200, R77, and alloys A-E with a diameter of 10 to 13 mm and a thickness of 1 or 2 mm were cut from a plain cylinder. CMSX-4 with a diameter of 20 mm and a thickness of 1–2 mm was cut as a semi-cylinder. Specimens as wrought 718, Ti-6Al-4V, and PM2000 with dimensions of 15 or 10×1 or 2 mm were cut from a plain ingot. All samples were ground to P600 grit surface finish. Each coupon was degreased in acetone and alcohol, then weighed before the oxidation test. The oxidation tests were conducted using SETARAM TAG24 S thermobalances. The samples were oxidized in a flow of synthetic air of 10 ml/min corresponding to a gas velocity of 0.53 mm/s at room temperature. The furnace was evacuated to primary vacuum before being filled with synthetic air. All heating rates and initial cooling rates were set at 60 °C/min. Data points were recorded every 10 s during the test.

Table 1 Chemical composition (wt%) of the metals and alloys

wt %	Ni	Fe	Cr	Al	Co	Mo	Ta	Ti	W	Nb	Hf	Re	C ppm	S ppm	Others
AMS20	Bal		4–5.5	5.4–6	5.5–7.5	0.1–0.7	7.5–9	0.1–0.25	4–5		0.04–0.15	4.8–6.2		8	
AMS20-S	Bal		4–5.5	5.4–6	5.5–7.5	0.1–0.7	7.5–9	0.1–0.25	4–5		0.04–0.15	4.8–6.2		< 1	
AMS19	Bal		4–5	5.9–6.5	9.5–10.5	0.3–0.7	7.5–8.5	0.2–0.7	3.2–4		0.1–0.2	3.7–4.5			
GOL1	Bal		4–8	6–8	12–15	0.5–3	4–6	0–3	0–2		0–0.2	3.5–5.5			
GOL2	Bal		6–9	4–6	5–8	2–4	5–7		2–5		0,1–0,9	5–7			
ST201	Bal		14.5–16.5	5–6.5	4.5–7	0–1.5	2–3.5	0–2	1–2.5		0–0.2				
CMSX-4	Bal		6.5	5.6	9	0.6	6.5	1	6		0.093	3	40	0.32	Mn 2.2 ppm
AM1	Bal		7.54	5.2	6.61	2.01	7.97	1.2	5.49		0.049	0.084	47	0.1	Mn 2 ppm
R77	Bal		14.6	4.3	15	4.2		3.35							
DS200	Bal		9	5	10			2	12.5	1	1.8				
IN 718	Bal	18	19	0.5	0.5	3.1	0.1	1		5.2			1000		Mn 0.2 Si 0.2
AD730	Bal	7.6	17.3	2.09	8.75	3.03		3.53		1.09					
IN 738	Bal		17.4	7.1	8.2	1	0.6	4	0.8	0.6			800		B 0.1 Zr 0.1
PM2000 (*Plansee*)		Bal	20	5.5				0.5							Y_2O_3 0.5
Cr *(Praxair)*			Bal												
Fe (*GoodFellow)*		Bal													
Ti6Al4V		0.16		6.4				Bal							V 3.5
Ni (*MRC)*	Bal														

Samples underwent stepwise multi-temperature thermogravimetric analysis (SMT-TGA). This testing procedure involves multiple steps and temperature dwells. The duration of each dwell is carefully selected to achieve optimal signal-to-noise ratio, aiming for approximately the same mass gain at each dwell. The mass gain rate should remain significantly higher than the drift of the TGA apparatus but not too large, allowing for several dwells without excessive oxidation of the sample. A specific temperature program was tailored for each alloy type, depending on the nature of the main oxide expected to form, such as NiO, FeO, TiO_2, Cr_2O_3 or Al_2O_3 (see Figure 1 and Supplementary information).

When a sample is oxidized at a given temperature after being oxidized at a succession of dwell at different temperatures, the microstructure of its oxide layer and the depletion profile of certain alloy elements in the metal are not the same as in simple isothermal oxidation. Therefore, the thermal history of the sample can influence its oxidation kinetics. To investigate potential effects of thermal history, such as the evolution of the parabolic constant over time or after high-temperature annealing of the oxide scale, the same temperature is used for two separate dwells in the SMT-TGA: one during temperature increase steps and the other during cooling steps. Effects of thermal history can then be identified by comparing kinetic parameters measured during the two dwells at the same temperature. If oxidation kinetics parameters remain similar across the two dwells, one may conclude the absence of history effects. Conversely, if oxidation kinetics parameters differ between the two dwells, a history effect is indicated.

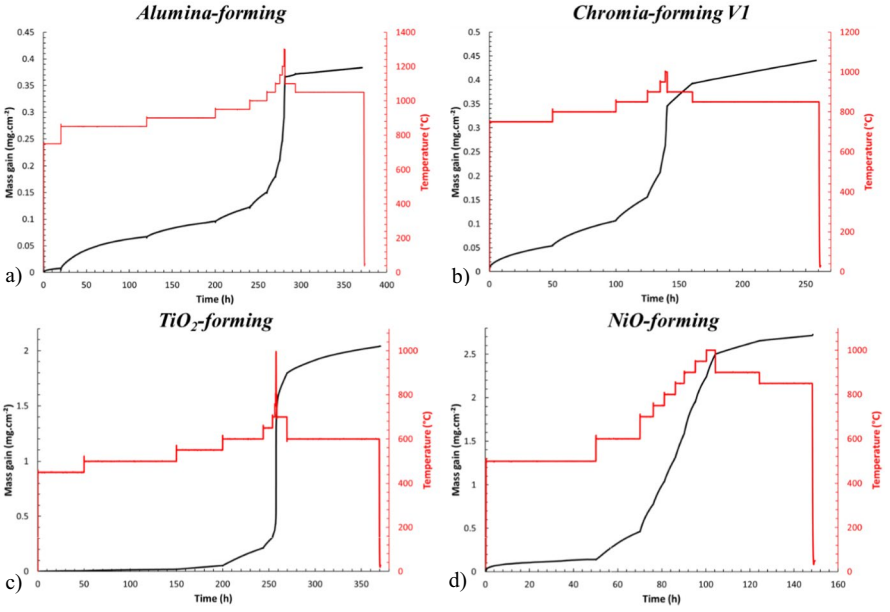

Fig. 1 Stepwise multi-temperature thermogravimetric analysis (SMT-TGA) programs for four types of materials, **a** alumina-forming alloys **b** chromia-forming alloys **c** Ti-alloys **d** NiO-forming alloys

Following each oxidation test, the oxide scale was examined using X-ray diffraction (not shown here) on a Bruker D8 GIXR instrument employing Cu-Kα radiation, with a step size of 0.02°, an angle of incidence of 10°, and a scan step time of 2 s within the 2θ range from 15° to 80°. Cross-sectional analyses were carried out using optical microscopy and a SEM FEI Quanta 450 equipped with a Bruker Quantax (SDD) EDS detector. EBSD analyses were employed to gain further insight into the microstructure of the oxide scale using a scanning electron microscope JEOL JSM-7100 equipped with a NordlyNano EBSD camera. To prevent any spallation of the oxide scale during cross-section polishing, the oxidized samples were coated with a thin layer of silver followed by an electroplated copper layer.

Results

Figure 2 presents the results of the SMT-TGA analysis on a commercial superalloy IN 718. The temperature program dedicated to the chromia-forming (v1) alloys was utilized. For each temperature dwell, the kinetic parabolic constant was calculated using the "complete parabolic law," as described in Eq. 1:

$$t = A + B \times \frac{\mathrm{dm}}{S} + \frac{1}{\mathrm{kp}} \times \left(\frac{\mathrm{dm}}{S}\right)^2 \tag{1}$$

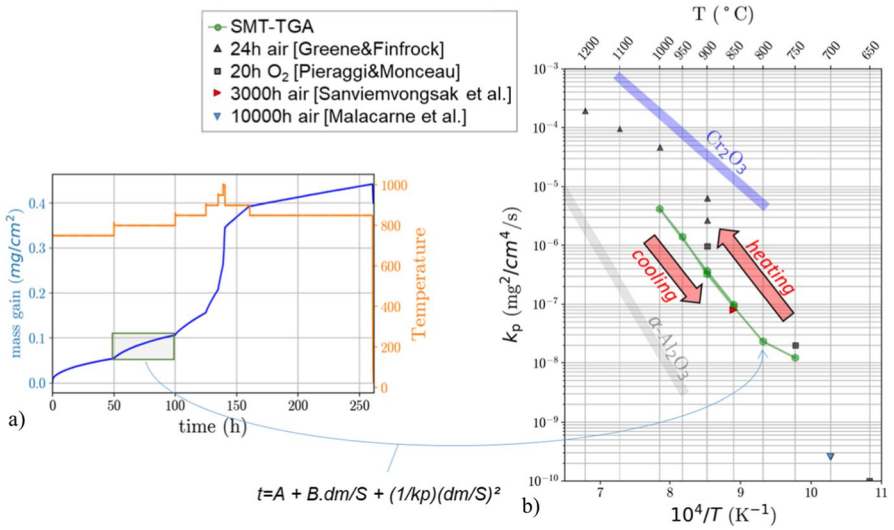

Fig. 2 Stepwise multi-temperature thermogravimetric analysis (SMT-TGA) of alloy 718 between 750 °C and 1000 °C in flowing dry air. **a** temperature program and mass change **b** resulting Arrhenius plot of parabolic constant k_p literature data from Greene et al. [15], Pieraggi et al. [13], Sanviemvongsak et al. [10]., and Malacarne et al. [14]

Indeed, it is not possible to calculate the parabolic constant k_p from the slope of $(dm/S)^2$ as a function of time t, as often observed in the literature. The use of the complete parabolic law is mandatory due to the oxide scale already formed before the high-temperature dwell [6]. The resulting values of k_p, for all the studied alloys, are given in the Supplementary information (Table 3 of annex for reviewing).

As the parabolic constant is calculated using the complete parabolic law (see Eq. 1), it is not necessary to correct the mass change curve to account for variations in Archimedean thrust due to temperature changes. However, it is possible to make this correction, for example, if one wishes to compare mass gain to oxide layer thickness at all points on the curve. For this purpose, a method has been proposed in [12] based on recording the mass during cooling at the end of the experiment.

For alloy 718, as shown in Fig. 2, it is evident that all values perfectly adhere to an Arrhenius law, except for the value at 750 °C, which is twice as high as expected from the extrapolation of values obtained at higher temperatures. The activation energy is calculated to be 297 kJ/mol between 800 and 1000 °C. Additionally, these values are in good agreement with previous results obtained from isothermal experiments conducted in our laboratory [10, 13] and they align with findings from Malacarne et al. [14] who studied very long-term oxidation at 700 °C. However, they are one order of magnitude lower than values reported by Green and Finfrock, who conducted 24-h oxidation at very high temperatures (900–1000 °C) [15]. This variance may be attributed to the discontinuous exposures performed by Green and Finfrock, coupled with the calculation of k_p using a simple parabolic law despite a transient regime of oxidation. Furthermore, our SMT-TGA results indicate that the values obtained at 900 °C and 850 °C after the dwell at 1000 °C closely resemble the values obtained at the same temperatures during the heating stage. This observation suggests the absence of an effect of thermal history for this alloy (718), at least for a thickness of the oxide scale between 1 and 3 µm (calculated from mass gain) and for a maximum temperature experienced of 1000 °C.

Figure 3 displays the results obtained with the titanium alloy Ti-6Al-4V. The aim of this study was to compare the oxidation kinetics of additive manufacturing Ti-6Al-4V by electron or laser power bed fusion (E-PBF or L-PBF) with a regular commercial rolled alloy. It is evident that all three alloys exhibit precisely the same oxidation behavior. Therefore, there is no discernible effect of the fabrication mode on the oxidation kinetics, despite significant differences in the alloy microstructures and the fact that a significant portion of the mass gain is attributable to oxygen dissolution in the alloy [7, 11]. From 450 to 1000 °C, the parabolic constant undergoes a substantial variation spanning 8 orders of magnitude. An "S-shape" curve can be observed between 450 °C and 800 °C in the Arrhenius plot. This phenomenon may stem from the combined effects of oxygen uptake for oxide scale growth and oxygen dissolution in the metal. At lower temperatures, mass gain primarily results from oxygen dissolution in the metal, while at higher temperatures, both scale growth and oxygen dissolution become significant factors. Casadebaigt et al. [16] have shown that oxygen dissolution in the Ti-6Al-4V alloy accounts for 15–20% of the total mass gain after 500 h at 600 °C, whereas it represents more than 80% after 2000 h at 500 °C. This hypothesis concerning the curvature of the curve in the Arrhenius plot

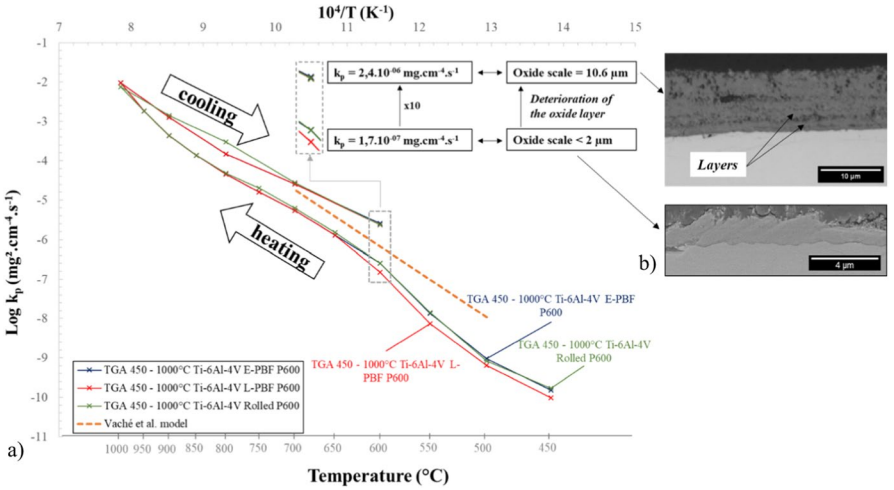

Fig. 3 Stepwise multi-temperature thermogravimetric analysis (SMT-TGA) of alloys Ti-6Al-4V between 450 °C and 1000 °C in flowing dry air. **a** Resulting Arrhenius plot of parabolic constant k_p **b** SEM cross-section images of oxide layer before and after high-temperature steps. Dotted red line: Vaché et al. model [17]

requires further analysis to be confirmed. Although the data points do not precisely align, they can be modeled by an approximate Arrhenius equation, revealing an apparent activation energy of 243 kJ/mol. These values can be compared to the model fitted to all available data in 2020 by Vaché et al. [17]. In Vaché et al., the activation energy is quite close with a value of 232 kJ/mol. Nevertheless, the k_P values from Vaché et al. are higher than the values calculated from kp evaluated with the SMT-TGA curve. This difference of a factor of 2–3 has been discussed in [17] and was attributed to the gas velocity which is much higher in Vaché et al. data (more than 1 m/s) than in thermogravimetry. Another clear feature of the Arrhenius plot is that the three alloys show higher values of k_p when cooling than during the heating steps. At 600 °C for example, there is an increase in more than one order of magnitude in the k_p ($2.4\ 10^{-6}$ instead of $1.7\ 10^{-7}$ $mg^2/cm^4/s$, see Fig. 3). This can be explained by the evolution of the microstructure of the oxide scale. In Fig. 3, it can be seen that the oxide scale is made of thin sublayers after the entire temperature program, whereas it is constituted of a single dense layer after an isothermal test of 500 h at 550 °C [7]. The layering of the oxide scale is well-documented [18] for titanium alloys, particularly for pure titanium and Ti-6Al-4V [7]. Upon closer examination of the Arrhenius plot in Fig. 3, a change in slope becomes evident for temperatures exceeding 900 °C. This may signify the onset of stratification within the oxide scale, accompanied by a partial loss of its protective properties. Conducting interrupted experiments with cross-sectional characterization would be necessary to validate this observation.

Discussion

SMT-TGA employs a single sample to measure parabolic rate constant k_p across a large range of temperatures, as opposed to utilizing multiple samples in separate isothermal tests. This approach minimizes experimental variations stemming from sample geometry or microstructure. The primary advantage of SMT-TGA lies in its efficiency in both time and material usage, particularly valuable during alloy development phases where material availability may be limited. However, it is important to note the potential for an effect of thermal history on the single sample between different tested temperatures, which can influence mass gains and consequently affect the estimation of kinetic parameters. This effect arises due to the dependency of oxidation rate on the microstructure of the oxide layer formed, which in turn is influenced by the sample's thermal history. Additionally, the nature of the oxide scale may evolve over time. A simple example of that is grain growth during oxidation of pure nickel [19] which leads to a decrease in the parabolic constant with time at constant temperature [19, 20]. To investigate this potential effect, the same temperature is applied during two separate dwells in the SMT-TGA—one during temperature rise and the other during cooling. Comparing the kinetic parameters measured during these dwells at the same temperature can help identify any history effect. It is not always easy to achieve because the mass gain rate decreases with the thickness of the oxide layer. It is therefore necessary to adjust the duration of the steps at the highest temperatures so that the mass gain during these steps is sufficiently limited. If this is not the case, it will indeed be impossible to measure the oxidation kinetics during the subsequent steps at lower temperatures. Furthermore, precautions should be taken to prevent "over-oxidization," ensuring the sample core remains unaffected by oxidation. Any oxide spallation or cracking induced by temperature changes should be monitored, with mass change measurements providing a precise indicator.

We thus propose various temperature programs for the different types of alloys. Numerical data will be provided (see Fig. 1 and Supplementary information Table 2) to facilitate the application of the SMT-TGA method and also allow for direct comparison of mass gain kinetics between different laboratories.

SMT-TGA offers a relatively rapid method for assessing the oxidation behavior of alloys across a broad temperature spectrum. To evaluate the reliability of SMT-TGA, classic isothermal thermogravimetry can be also performed for comparison. This was done for example with the AM1 alloy, nine conventional isothermal TGA tests were also conducted at various temperatures ranging from 800 °C to 1200 °C. They are described in [9]. A first database was created with oxidations under synthetic air flow and the same surface condition for all samples (ground P600). Pure metals were tested: Ni, Fe, Cr, and commercial alloys from different families such as alloy a common Ti-alloy Ti-6Al-4V, chromia-forming alloys 718, AD730, DS200, and the alumina-formers PM2000, CMSX-4 and AM1. All these mass gain results and parabolic constants will be made available (Supplementary Information). New alloys under development have also been tested and

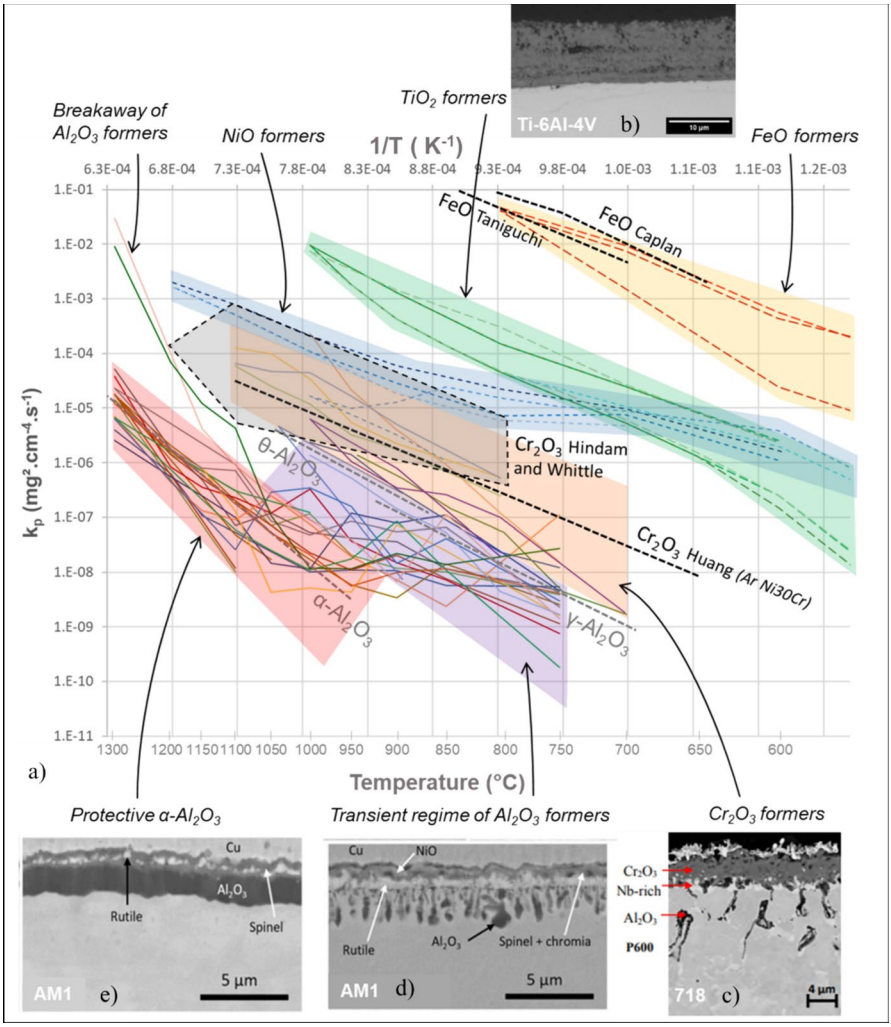

Fig. 4 Kinetics data with stepwise multi-temperature thermogravimetric analysis (SMT-TGA) to classify alloys. **a** Arrhenius diagram, SEM cross-section image: **b** Ti-6Al-4V **c** 718 alloy, **d** Transient regime of AM1, e) α-Al_2O_3 regime of AM1. Bibliographic data from Brumm et al. on NiAl [21], Huang et al. [22], Hindam et al. [23], Caplan et al. [24], and Taniguchi et al. [25]

are not detailed here. Figure 4 compiles these results into an Arrhenius diagram, which allows for the direct comparison of oxidation kinetics of the different alloy families at all temperatures. From the fastest to the slowest mass gain kinetics, we find the oxidation of iron, titanium, nickel, chromino-forming alloys, and alumina-forming alloys. This diagram is created in the spirit of the famous review by Hindam and Whittle. [23]. We notice possible variations of one order of magnitude for the same alloy, even for pure metals, depending on the microstructure of the oxide layer; and variations of two orders of magnitude between different

chromino-forming alloys or different alumina-forming alloys. This could be due to the microstructure of the oxide layers but also to the presence of reactive elements [26]. It is remarkable that all alumina-forming alloys tested exhibit, below 1000–1050 °C, oxidation kinetics much higher than those corresponding to the growth of alpha alumina. These alloys exhibit a transient oxidation regime in which the kinetics may be controlled by the growth of transition alumina [21] or by the growth of chromia or spinels [23], and it is worth noting that this transient regime can be very long and last throughout the application life of the alloy [9].

Conclusions

SMT-TGA has emerged as a potent and easily applicable technique, enabling the acquisition of oxidation kinetics across a broad temperature spectrum using just a single sample. Consequently, it serves as a valuable tool for assessing new materials, particularly in scenarios where material and time resources are limited for testing each new alloy grade. In the case of Ti-6Al-4V alloy, it proved highly efficient in demonstrating the absence of additive manufacturing effects on oxidation kinetics. Similarly, for superalloy AM1, it provided a rapid means to identify and quantify the presence of a transient oxidation regime below 1050 °C. It is worth noting that the same method can also be utilized in conjunction with thermal cycling [27] or to simulate flight programs. However, caution should be exercised in designing the temperature program and interpreting the results.

Supplementary Information The online version contains supplementary material available at https://doi.org/10.1007/s11085-024-10273-8.

Acknowledgements The tests and the analyses were carried out at the CIRIMAT laboratories with the financial support a different partnership contracts with Safran and IRT St-Exupery. The alloys were supplied by Safran and IRT St-Exupery.

Author Contribution Daniel Monceau involved in original idea, conceptualization, experimental design, running some experiments, and writing of the first draft. Hugo Enjalbert, Thomas Perez, and Antoine Casadebaigt involved in sample preparation and running some experiments; Hugo Enjalbert and Clara Desgranges involved in preparing figures. Hugo Enjalbert prepared all tables. All authors discussed the results and reviewed the manuscript.

Funding Open access funding provided by Institut National Polytechnique de Toulouse.

Data Availability Data are provided within the manuscript and supplementary information files. They are available upon request at daniel.monceau@toulouse-inp.fr.

Declarations

Conflict of interest The authors declare that they have no known competing financial interests or personal relationships that could have appeared to influence the work reported in this paper.

References

1. D. G. Backman, D. Y. Wei, D. D. Whitis *et al., JOM* (2006), 36–41
2. W. Yi Wang, J. Li, W. Liu *et al., Computational Materials Science* **158**, (2019), 42–48
3. S. Gravier, M. Coulombier, A. Safi, et al., *J. Microelectromech. Syst.* **18**, 2009 (555).
4. A. I. Mardare, A. Savan, A. Ludwig, et al., *Corrosion Science* **51**, 2009 (1519).
5. W. D. Summers, D. L. Poerschke, M. R. Begley, et al., *Journal of the American Ceramic Society* **103**, 2020 (5196).
6. D. Monceau and B. Pieraggi, *Oxidation of Metals* **50**, 1998 (477).
7. A. Casadebaigt, PhD thesis, University of Toulouse (2020).
8. T. Sanviemvongsak, PhD thesis, University of Toulouse (2020).
9. T. Perez, D. Monceau, and C. Desgranges, *Corrosion Science* **206**, 2022 (110485).
10. T. Sanviemvongsak, D. Monceau, and B. Macquaire, *Corrosion Science* **141**, 2018 (127).
11. A. Casadebaigt, J. Hugues, and D. Monceau, *Oxidation of Metals* **90**, 2018 (633).
12. D. Monceau and D. Poquillon, *Oxidation of Metals* **61**, 2004 (143).
13. D. Monceau and B. Pieraggi, *Oxidation kinetics of alloy 718 in 1atm O2 studied by thermogravimetry, unpublished results* (1998)
14. R. Malacarne, S. Mathieu, L. Aranda, et al., *Corrosion Science* **188**, 2021 (109500).
15. G. A. Greene and C. C. Finfrock, *Oxidation of Metals* **55**, 2001 (505).
16. A. Casadebaigt, J. Hugues, and D. Monceau, *Corrosion Science* **175**, 2020 (108875).
17. N. Vaché, Y. Cadoret, B. Dod, et al., *Corrosion Science* **178**, 2021 (109041).
18. J. Stringer, *Acta Metallurgica* **8**, 1960 (758).
19. A. Atkinson, R. I. Taylor, and A. E. Hughes, *Philosophical Magazine A* **45**, 1982, 823–833
20. R. Peraldi, D. Monceau, and B. Pieraggi, *Oxidation of Metals* **58**, 2002, 275–295
21. M. W. Brumm and H. J. Grabke, *Corrosion Science* **33**, 1992, (1677).
22. X. Huang, L. Martinelli, S. Bosonnet, et al., *High Temperature Corrosion of Materials* **100**, 2023 (745).
23. H. Hindam and D. P. Whittle, *Oxidation of Metals* **18**, 1982 (245).
24. D. Caplan, G. I. Sproule, and R. J. Hussey, *Corrosion Science* **10**, 1970 (9).
25. S. Taniguchi and D. L. Carpenter, *Corrosion Science* **19**, 1979 (15).
26. W. T. Griffiths and L. B. Pfeil, *Improvements in heat resistant alloys,* Patent **GB459848A** (1937)
27. F. Nozahic, D. Monceau and C. Estournès, *Materials & Design* **94**, 2016, 444–448